arXiv:2508.12966v1 [cs.CV] 18 Aug 2025

GazeDETR: Gaze Detection using Disentangled Head and Gaze Representations

Ryan Anthony Jalova de Belen
University of New South Wales
ryanxdebelen@gmail.com

Gelareh Mohammadi

Arcot Sowmya

Abstract

*Gaze communication plays a crucial role in daily social interactions. Quantifying this behavior can help in human-computer interaction and digital phenotyping. While end-to-end models exist for gaze target detection, they only utilize a single decoder to simultaneously localize human heads and predict their corresponding gaze (*e.g.*, 2D points or heatmap) in a scene. This multitask learning approach generates a unified and entangled representation for human head localization and gaze location prediction. Herein, we propose GazeDETR, a novel end-to-end architecture with two disentangled decoders that individually learn unique representations and effectively utilize coherent attentive fields for each subtask. More specifically, we demonstrate that its human head predictor utilizes local information, while its gaze decoder incorporates both local and global information. Our proposed architecture achieves state-of-the-art results on the GazeFollow, VideoAttentionTarget and ChildPlay datasets. It outperforms existing end-to-end models with a notable margin.*

1. Introduction

Gaze allows humans to communicate information and share intentions effectively. In addition, gaze direction can be used to evaluate another person's interest in the environment. The task of identifying humans and their gaze locations can be formulated as a prediction problem of a set <*Human, Interaction, Gaze Target*> [6, 29]. The successful development of computational models that can automatically solve this problem is beneficial for numerous practical applications, including human-robot interaction [1, 15], social interaction analysis [8] and digital phenotyping of behaviors for mental health diagnosis [6, 7, 17, 24]. Earlier approaches required human bounding box locations to predict the gaze target [4, 5, 23, 25, 26]. Recently, end-to-end approaches have employed transformer architectures and utilized a multitask learning approach to predict human head locations and their corresponding gaze locations simultaneously[6, 29].

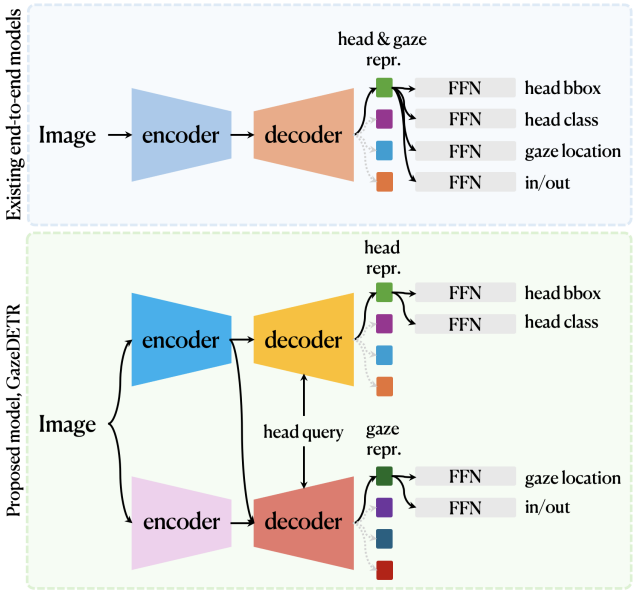


Figure 1. Comparison of existing approaches and the proposed approach (GazeDETR) for end-to-end gaze target detection. *(top)* existing approaches learn a unified representation for human head localization and gaze target detection, while *(bottom)* GazeDETR learns disentangled representations for the two subtasks. A shared query is used to promote interactions between the two decoders.

As shown in Figure 1 *(top)*, recent transformer-based approaches leverage the embeddings of a single decoder to learn joint representations necessary for the multi-task learning of gaze target detection [6, 19, 29]. Each embedding is used in any of the following: determination of a human head location, identification of the corresponding gaze location (through heatmap prediction or direct regression of gaze location), classification of the gaze interaction (*e.g.*, looking or not looking) and prediction of whether the gaze target is inside or outside the frame. These tasks require different (and sometimes conflicting) information to perform optimally. For example, human head localization requires local information, while gaze location prediction necessitates a mixture of local and global information to identify complex interactions.



Figure 2. Cross-attention of the head predictor and gaze decoder. The predictions (blue) and ground truth (orange) are also shown.

To alleviate the heavy reliance on a single decoder to perform these subtasks, we propose GazeDETR, a transformer-based architecture that follows a parallel decoding process and disentangles the representation learning of head localization and gaze location prediction, as shown in Figure 1 *(bottom)*. The embeddings after the first decoder are used to identify human head locations, while the embeddings after the second decoder are used for gaze location prediction and gaze interaction (*e.g.*, in vs out) classification.

Compared to existing end-to-end models, GazeDETR is conceptually similar to traditional methods that consist of a head branch and a scene branch. GazeDETR comprises three components: (1) a human head predictor learns to incorporate local information to identify the location of human heads, (2) a scene feature encoder aims to capture long-range dependencies between the human head and scene through feature fusion, and (3) a gaze decoder identifies corresponding gaze locations using the combined features.

The success of the two decoders (*e.g.* head predictor and gaze decoder) relies on the effective formulation of the attention layers of the transformer architectures. In particular, the cross-attention maps of the human head predictor need to precisely localize the human heads. For the gaze decoder, the self-attention maps need to initially incorporate head information, while the cross-attention maps should highlight the head and salient areas that may attract attention to identify the final gaze location. Figure 2 shows a multi-person scene, where GazeDETR successfully detects humans and their gaze. It achieves coherent attention maps through careful design considerations that will be described in detail. This paper makes the following contributions:

1. we present gazeDETR, an end-to-end model that disentangles representations necessary for human head localization and gaze target detection.
2. we report new state-of-the-art results across different metrics on three evaluation benchmarks.

2. Related Work

Gaze target detection is defined as the task of predicting the focus of attention of a specific person [23]. The focus of attention is represented either as a probability distribution (*i.e.* a gaze heatmap that indicates high-intensity values for areas of high focus of attention) or an exact location (*i.e.* x and y coordinates). Gaze target detection has later been extended to include a binary classification task to determine whether the person is looking at a location inside or outside the frame [5]. While there are numerous applications of gaze target detection to different input (*e.g.* video, VR [2]), this paper focuses on gaze target detection in images.

Existing solutions to gaze detection can be broadly categorized into two, namely multi-branch and end-to-end models. Multi-branch approaches follow the original problem formulation in which gaze locations of specific humans are predicted, while the end-to-end approaches aim to jointly predict all human head locations and their corresponding gaze locations. This means that multi-branch approaches require an input image and the location of human heads, whereas end-to-end approaches only need an input image.

Multi-branch models. Most traditional methods follow a two-branch architecture in which the first branch uses the entire image to determine salient regions that may attract human attention, while the second branch requires a human head location to infer the gaze direction [4, 5, 9, 14, 15, 18, 23, 25, 26]. Other methods utilize a multi-stream architecture that combines different information (*e.g.* pose and depth) for improved feature learning [9, 11]. Fusion mechanisms are then incorporated to determine the gaze location. These methods require human head locations acquired through either a laborious manual annotation or high-performing off-the-shelf head detectors. Multiple forward passes are then performed to identify the gaze locations of the identified humans in the image.

End-to-end models. To achieve a single forward pass for multi-person gaze location detection, recent approaches utilize transformer-based architectures. Existing gaze detection models take an input image and jointly predict the human head locations and their corresponding gaze [6, 28, 29]. These are inspired by DEtection TRansformers (DETR) [3, 20, 22] that formulate object detection as a set prediction problem. However, existing end-to-end gaze models use a single decoder that learns a unified and entangled representation that aggregates features for human head localization and gaze target detection. This representation results in inconsistent attentive fields for each subtask.

To address this, we present GazeDETR, an end-to-end architecture comprising two disentangled decoders that learn separate representations that are specialized for each subtask (*e.g.*, human head localization and gaze prediction). We demonstrate that GazeDETR achieves superior performance across different benchmarks.

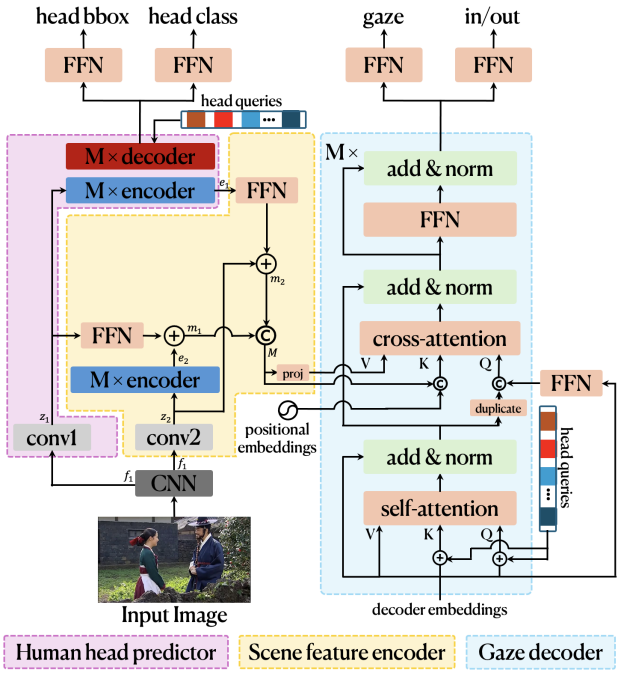


Figure 3. GazeDETR overview. The human head predictor extracts relevant features from the input image for head localization. Additional contextual information is extracted using the scene feature encoder and used by the gaze decoder for gaze prediction.

3. GazeDETR Architecture

The proposed GazeDETR architecture is shown in Figure 3. It consists of three main components: (1) human head predictor, (2) global scene feature encoder, and (3) gaze decoder. The human head predictor aims to identify all the bounding box locations of human heads in the scene. The global scene feature encoder aims to combine human head and scene features that are necessary in identifying the gaze directions. Finally, the gaze decoder is conditioned using the learned human head queries of the human head decoder.

3.1. Motivation

Existing end-to-end architectures [6, 29] define gaze target prediction as a set prediction problem, inspired by DETR. Similar to object detection, each prediction consists of head location, a target of attention, and a binary classification of interaction type (*e.g.*, looking or not looking). While they have been shown to exhibit promising performance, these architectures only contain a single decoder trained with learnable queries for multi-task prediction. Because these queries need to incorporate local information for human head localization and global scene information for gaze detection, their overall performance is impacted by the need to learn these features by only using a single decoder. In this work, two separate decoders are used to predict the human head locations and identify their corresponding gaze targets.

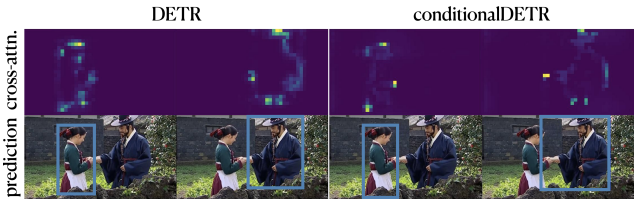


Figure 4. Visualization of the cross-attention maps of DETR architectures. Both DETR [3] and conditionalDETR [22] generate maps that highlight the extremities of the detected objects.

3.2. Human head predictor

The architecture of the human head predictor is similar to other DETR-like architectures [3, 20, 22]. As shown in Figure 3 (purple region), it consists of an image feature extractor (*e.g.* CNN) backbone, a transformer encoder, a transformer decoder and FFNs that predict the binary class (*e.g.* human or not human) and bounding box locations. First, the backbone extracts feature representations $f_1 \in \mathbb{R}^{C\times H\times W}$. A 1×1 convolution operation is then applied to reduce the feature dimension to a smaller dimension d, resulting in a feature map $z_1 \in \mathbb{R}^{d\times H\times W}$. This feature map is enriched using a transformer encoder into $e_1 \in \mathbb{R}^{d\times H\times W}$ and passed to a transformer decoder whose embeddings are finally passed to separate FFNs for human box regression and classification. The spatial queries (p_q) of the decoder are learned positional encodings that contain spatial priors (*e.g.* box center coordinates, width and height) about the human heads. GazeDETR utilizes these spatial queries in its gaze decoder for more accurate gaze prediction.

3.3. Global scene feature encoder

As shown in Figure 4, DETR-like architectures [3, 22] used for object detection enable the prediction of humans in the scene. However, a closer examination of their decoder layers reveals that the cross-attention maps attend to the extremities. This observation suggests that utilizing the same decoder embeddings learned for human head localization is problematic for gaze direction prediction because they lack contextual information. To identify the gaze directions more effectively, a separate encoder must learn a disentangled representation that contains relevant visual context and captures global information. As shown in Figure 3 (yellow region), a separate 1×1 convolution operation is applied to f_1, resulting in a $z_2 \in \mathbb{R}^{d\times H\times W}$. Similar to the human predictor, z_2 is enriched using a transformer encoder into $e_2 \in \mathbb{R}^{d\times H\times W}$. To enable better feature fusion between the two encoders, z_1 is linearly projected and added to e_2 while e_1 is linearly projected and added to z_2, resulting in m_1 and m_2 respectively. Finally, these two features are linearly concatenated feature-wise to form a global memory $M \in \mathbb{R}^{2d\times H\times W}$ to be used by the gaze decoder.

3.4. Gaze decoder

Unlike the human head predictor whose spatial queries p_q are learnable and randomly initialized, the gaze decoder uses the p_q from the human head predictor as its spatial query. These p_q are utilized in both the self- and cross-attention layers of the gaze decoder to leverage the spatial priors of the human heads learned during training.

Self-attention. The self-attention layers aim to enrich the embeddings of the previous decoder layers so they can be used to effectively identify the gaze locations of the human heads in the scene. The decoder embeddings at the first layer (E_0) are initially set to zero. The self-attention layers of a vanilla transformer decoder architecture form the keys and queries by adding the previous decoder embeddings, E_{i-1}, with a learnable query. Instead of using a learnable query that is randomly initialized, the self-attention layers of GazeDETR utilize p_q, the spatial query of the human head predictor, during the formation of its keys and queries.

$$\begin{aligned} K_i &= W^{K_E} E_{i-1} + W^{K_p} p_q \\ Q_i &= W^{Q_E} E_{i-1} + W^{Q_p} p_q \end{aligned} \tag{1}$$

W are projection matrices. Compared to utilizing randomly initialized queries, directly using p_q guides the gaze decoder to concentrate on human heads in the self-attention layers.

Cross-attention. To further utilize human head information, in the first cross-attention layer, the p_q is added to the output of the self-attention layer. The key is formed by concatenating (1) the global memory M that contains human head and scene features and (2) the positional encoding p_k.

$$\begin{aligned} K &= concat([W^{K_M} M, W^{K_p} p_k]) \\ &= concat([W^{K_M} m_1, W^{K_M} m_2, W^{K_p} p_k])) \end{aligned} \tag{2}$$

The query is formed by concatenating the self-attention output c_q twice and the previous decoder embeddings E_{i-1}.

$$Q = concat([W^{Q_c} c_q, W^{Q_c} c_q, W^{Q_E} E_{i-1}]) \tag{3}$$

Removing the weight matrices for brevity, the resulting cross-attention consists of the following terms:

$$c_q^T m_1 + c_q^T m_2 + E_{i-1}^T p_k \tag{4}$$

Finally, the value (V) is formed by projecting the global M from $2d$ back to d dimension. Note that Equation (4) and V influence the final decoder embeddings used to identify the gaze locations. In our reformulation of cross-attention, the first two terms of Equation (4) promote separate yet effective interaction between the c_q and the human head m_1 and scene features m_2 to accurately identify the gaze locations. The concatenation of m_1 and m_2 is deliberate since the addition operation fails to ensure such interactions. The last term allows the decoder to exploit its previous embeddings, as compared to learning p_q from scratch.

3.5. Loss Calculation

Similar to other DETR-like architectures, the loss calculation is composed of two stages: (1) the bipartite matching and (2) the loss calculation for model training.

Bipartite matching. We use the Hungarian algorithm [16] to obtain the optimal matching between the ground truth and the model predictions. The matching cost is defined as:

$$\mathcal{L}_{cost} = \sum_{i}^{N_q} \mathcal{L}_{match}(t^i,) \tag{5}$$

The matching cost $\mathcal{L}_{match}$ consists of: (1) binary human head class $\mathcal{L}_h$ and (2) the human head location $\mathcal{L}_{bbox}$. The $\mathcal{L}_{head}$ is calculated using focal loss. $\mathcal{L}_{bbox}$ is defined as the sum of the L1 loss and the generalized intersection-over-union (GIoU) loss during the box regression task.

$$\mathcal{L}_{bbox} = \alpha_1 \left\| t_i^b - o_{w(i)}^t \right\| - \alpha_2 GIoU(t_i^b, o_{w(i)}^t) \tag{6}$$

Loss function. Once the bipartite matching between the ground truth and the model predictions has been achieved, the loss function is computed as follows:

$$\begin{aligned} \mathcal{L}_{cost} = \alpha_1 \mathcal{L}_{bbox} + \alpha_2 \mathcal{L}_{class} + \alpha_3 \mathcal{L}_{in\_out} \\ + \alpha_4 \mathcal{L}_{gaze} + \alpha_5 \mathcal{L}_{heatmap} \end{aligned} \tag{7}$$

where $\mathcal{L}_{in\_out}$ is the binary cross entropy loss, $\mathcal{L}_{gaze}$ is the L1 loss between the ground truth and gaze predictions, and $\mathcal{L}_{heatmap}$ is the L2 distance between the ground truth and heatmap predictions.

In our experiments, we found that adding $\mathcal{L}_{in\_out}$, $\mathcal{L}_{gaze}$ and $\mathcal{L}_{heatmap}$ to the bipartite matching resulted in overlapping human head predictions but different gaze directions. This explains why the cost functions for the bipartite matching and loss optimization are different. More information can be found in our ablation studies in Section 4.4.

4. Experiments

4.1. Datasets and Evaluation Metrics

Datasets. GazeDETR was trained and evaluated on three datasets. *GazeFollow* [23] is a large-scale dataset consisting of a training set of 122k images with 130k annotated gaze instances and a test set comprising a total of 4782 instances. The original annotations include head bounding boxes and the corresponding 2D gaze points. An extension was made to include a binary label indicating whether the gaze target is inside or outside the frame. *VideoAttentionTarget* [5] is a dataset consisting of 1,331 high-resolution videos collected from 50 popular TV shows, resulting in 71k frames with 164k gaze instances. Similar to the *GazeFollow* dataset, the annotations include the head bounding boxes, 2D gaze points and binary in/out labels. *ChildPlay* [25] is a dataset

focused on analyzing gaze behaviors of children engaged in play activities with adults. It consists of 401 video clips extracted from 95 videos uploaded on YouTube, resulting in 120k frames with a total of 257k gaze instances. The annotations follow the same protocol as the previous datasets.

Various image augmentation was used during training. In particular, input images were resized to a resolution of at least 480 pixels and at most 800 pixels in height and at most 1333 pixels in width. A random flip and crop was applied with a probability of 0.5. Each batch was ensured to have the same size by appending zeros to the shorter side of each sample. To avoid overfitting in the video datasets, each clip was sampled every 5 frames during training.

Evaluation Metrics. GazeDETR jointly predicts the human head locations and their associated gaze locations, requiring the need to evaluate its performance on both human head localization and gaze location detection.

For human head localization, the commonly used mean average precision (*mAP*) was used [29]. A human head is considered a true positive if and only if the model correctly identifies and localizes the human head (*e.g.* intersection over union (IoU) value between the predicted human head location and the ground truth is greater than 0.5). In addition, the associated gaze location should be correctly predicted (*e.g.* the L_2 distance between the predicted gaze coordinates and the ground truth is less than 0.15).

For gaze location detection, three standard metrics [5, 23] were used: (1) area under the ROC curve (*AUC*) (2) *Distance* (3) *Average Precision*. For the *AUC*, the predicted heatmap was evaluated at different thresholds in the ROC curve. Depending on the dataset, the *Minimum Distance*, *Average Distance* and/or L_2 *distance* are reported for the *Distance* metric. The L_2 distance was computed between the gaze target prediction and ground truth. The *Average Distance* is the Euclidean distance between the model prediction and the average of the ground truth gaze locations. The *Minimum Distance* was chosen to be the minimum distance calculated from the set of pairwise distances between the model prediction and ground truth gaze locations. Finally, the *Average Precision* was used to evaluate the model performance in gaze interaction (in vs out) classification.

4.2. Implementation Details

The proposed architecture consists of three components:

- Similar to other DETR-like architectures, the human head predictor contains an image feature extractor (ResNet-50 [12]), a 1×1 convolutional layer, a six-layer transformer encoder, a six-layer transformer decoder and two feedforward networks that transform the decoder embeddings to the human head bounding box locations and binary human head class. This predictor learns 100 queries, allowing it to detect 100 human heads in an image.
- The global scene feature encoder consists of a 1×1 convolutional layer and a six-layer transformer encoder. It enriches the features from the image feature extractor, learns projection matrices and integrates the learned embeddings of the human head predictor to form the global memory for the gaze decoder.
- Finally, the gaze decoder consists of a 6-layer transformer decoder that performs self-attention on the decoder embeddings. Afterwards, it performs cross-attention between the global memory M and the self-attention output. The decoder embeddings are finally transformed into gaze locations using a three-layer FFN.

All transformer layers employ Xavier initialization [10], with a dropout rate of 0.1. There are 8 multi-head attention for the self- and cross-attention transformer layers. AdamW optimizer [21] is used. The weight decay is set to 10^{-4}. The learning rates for the backbone and the transformer are initially set to be 10^{-5} and 10^{-4}, respectively. GazeDETR was trained from scratch on *GazeFollow* and fine-tuned on *VideoAttentionTarget* and *ChildPlay* with learning rates 10^{-6} for the backbone and 10^{-5} for the transformers.

4.3. Comparison with the State-of-the-Art

Quantitative comparison between GazeDETR and existing models trained on *GazeFollow* and *VideoAttentionTarget* are reported in Table 1, while evaluation on *ChildPlay* is reported in Table 2. The top section of both tables requires human head locations as input; hence mAP results are not reported. The bottom section contains existing end-to-end gaze target detection models, with mAP evaluation. GazeDETR achieved new state-of-the-art results across all metrics in all 3 datasets, a notable leap, especially in terms of the performance of end-to-end gaze detection models.

Compared to existing multi-branch models, GazeDETR yielded an almost 1% improvement in AUC. It achieved a lower average distance (0.101 vs 0.113) and minimum distance (0.055 vs 0.056) on *GazeFollow*. It also achieved a lower L2 distance and better AP performance when compared to the leading model trained on *VideoAttentionTarget*. A similar observation may be made on *ChildPlay*.

Compared to existing end-to-end models for gaze prediction, GazeDETR achieved higher performance across all metrics, especially in terms of AUC, L2 distance and mAP. It is worth noting that there was almost a 4% AUC improvement when compared to HGTTR on the GazeFollow dataset. It also achieved a notably lower L2 distance (0.098 vs 0.137) and a significant gain of 17.3 mAP compared with HGTTR on the *VideoAttentionTarget* dataset.

Despite being an end-to-end model, GazeDETR consistently outperformed existing models across all datasets. We attribute its performance to the careful design of its components that aim to disentangle representations of human head localization and gaze target prediction.

Method	GazeFollow				VideoAttentionTarget			
	AUC ↑	Avg. Dist ↓	Min. Dist ↓	mAP ↑	AUC ↑	Dist ↓	AP ↑	mAP ↑
Recasens [23]	0.878	0.190	0.113	—	—	—	—	—
Chong [4]	0.896	0.187	0.112	—	0.830	0.193	0.705	—
Lian [18]	0.906	0.145	0.081	—	0.837	0.165	—	—
Chong [5]	0.921	0.137	0.077	—	0.860	0.134	0.853	—
Fang [9]	0.922	0.124	0.067	—	0.905	0.108	0.896	—
Jin [15]	0.920	0.118	0.063	—	—	0.109	**0.897**	—
Tonini [27]	0.927	0.141	—	—	—	0.129	—	—
Gupta [11]	0.943	0.114	0.056	—	—	0.110	0.879	—
Bao [2]	0.928	0.122	—	—	—	0.120	0.869	—
Hu [13]	0.923	0.128	0.069	—	—	0.118	0.881	—
Tafasca [25]	0.936	0.125	0.064	—	—	0.109	0.834	—
Jin [14]	0.919	0.126	0.076	—	—	0.134	0.880	—
Sharingan [26]	0.944	0.113	0.057	—	—	0.107	0.891	—
HGTTR [29]	0.917	0.133	0.069	0.547	0.893	0.137	0.821	0.514
gazeDETR (Ours)	**0.952**	**0.101**	**0.055**	**0.548**	**0.907**	**0.098**	**0.897**	**0.687**

Table 1. Quantitative results of different models on the GazeFollow and VideoAttentionTarget datasets. The first section of the table includes existing models that require human bounding box locations as input, while the second section includes end-to-end models that include mAP for human head localization performance. Best scores are reported in **bold**.

Method	AUC ↑	Dist ↓	AP ↑	mAP ↑
Gupta [11]	—	0.113	0.983	—
Tafasca [25]	—	0.107	0.986	—
Sharingan [26]	—	0.106	0.990	—
gazeDETR (Ours)	0.872	**0.085**	**0.993**	0.654

Table 2. Quantitative comparison on the ChildPlay dataset.

#	Module		Performance Metrics			
	GSFE	New p_q	AUC ↑	A.D. ↓	M.D. ↓	mAP ↑
A	✗	✗	0.928	0.122	0.073	0.493
B	✗	✓	0.946	0.106	0.059	0.521
C	✓	✓	0.950	0.103	0.056	0.527
D	✓	✗	**0.952**	**0.101**	**0.055**	**0.548**

Table 3. The performance metrics of GazeDETR variants with different module combinations (GSFE: Global Scene Feature Encoder, New p_q denotes a unique query instead of the head query).

4.4. Ablation Study

Several GazeDETR variants were explored to validate the effectiveness of the global scene feature encoder (GSFE) and the learnable spatial query of the gaze decoder. Note that the human head predictor cannot be removed because it breaks the end-to-end pipeline. Various training paradigms (*e.g.*, bipartite matching strategy and loss components) and model parameters (*e.g.*, backbone and number of head queries and decoder layers) were also explored. All variants were trained and evaluated on *GazeFollow*.

Shared Encoder. The GSFE was removed to illustrate its usefulness. GazeDETR variants A and B in Table 3 were trained using a shared encoder between the human head predictor and the gaze decoder. The encoded features, e_1, learned by the human head predictor were used as the global memory of the gaze decoder. In this variant, the key in the cross-attention layers of the gaze decoder was formed by concatenating e_1 and the positional encoding. The query was formed by concatenating the decoder embedding and the spatial query. Finally, the value was formed by linearly projecting e_1. As previously illustrated, DETR-like models for object detection generate cross-attention maps that localize the detected object. Directly utilizing the encoded features of the human head predictor (variants A,B) resulted in the lowest performance across all metrics, as shown in Table 3. This observation can be attributed to the fact that gaze prediction requires global information. Learning separate global information using the GSFE (variants C,D) resulted in an observable increase in performance, highlighting the importance of GSFE for gaze detection.

Learnable Gaze Query. GazeDETR variants B and C were trained using a separate learnable 'gaze' query (randomly initialized) for the gaze decoder. As shown in Table 3, these variants resulted in a 2% decrease in the mAP, suggesting that the head queries learned by the human head predictor encode spatial information that helps the gaze decoder identify corresponding gaze targets of the predicted heads. In the next ablations, GazeDETR variant D was used due to its superior performance across all metrics.

#	Loss Component		Gaze Prediction Output		Performance Metrics			
	Head Local.	Gaze Pred.	Gaze Location	Heatmap	AUC ↑	Avg. Dist ↓	Min. Dist ↓	mAP ↑
BM1	✓	✗	✓	✗	0.952	**0.101**	**0.055**	**0.548**
BM2	✓	✗	✗	✓	0.782	0.303	0.234	0.072
BM3	✓	✗	✓	✓	**0.969**	0.109	0.062	0.184
BM4	✓	✓	✓	✗	0.932	0.121	0.069	0.493
BM5	✓	✓	✗	✓	0.783	0.292	0.225	0.070
BM6	✓	✓	✓	✓	0.962	0.117	0.068	0.488

Table 4. Performance metrics of GazeDETR variants with different bipartite matching loss components and gaze prediction outputs.

#	$\#p_q$	#Dec.	Performance Metrics			
			AUC↑	A.D.↓	M.D.↓	mAP↑
Q1	20	6	0.932	0.121	0.071	0.440
Q2	50	6	0.951	0.102	0.056	0.512
Q3	100	2	0.948	0.103	0.058	0.521
Q4	100	4	0.951	0.104	0.057	0.516
Q5	100	6	**0.952**	**0.101**	**0.055**	**0.548**

Table 5. Performance metrics of GazeDETR variants with different numbers of head queries and decoder layers.

Bipartite Matching Strategy and Loss Components. Our proposed bipartite matching strategy consists of different loss components associated with human head localization and gaze prediction. The gaze prediction output is commonly optimized to accurately predict a gaze heatmap, a gaze location (*e.g.* x and y coordinates) or both. Note that the in/out prediction is always included regardless of the gaze prediction output. As shown in Table 4, experimental results revealed that GazeDETR variants BM2 and BM5 that predicted only a heatmap achieved the lowest performance regardless of the bipartite matching strategy used. Directly regressing only the gaze location (variants BM1, BM4) or combining regression and heatmap prediction (variants BM3, BM6) resulted in similar performances in terms of both distance metrics. GazeDETR variants with an additional heatmap prediction output (variants BM3, BM6) achieved the highest AUC performance, which is expected due to heatmap supervision during training. Finally, we note that the highest-performing model, BM1, only included the head localization during bipartite matching. We observe that adding the gaze prediction output in the bipartite matching strategy resulted in the same human head with different gaze predictions, negatively impacting the mAP performance in variants BM4, BM5 and BM6.

Number of Head Queries and Decoder Layers. As shown in Table 5, GazeDETR performance increases across all metrics, with the mAP improving significantly as the number of queries increases. A similar effect was found as the number of decoder layers increased.

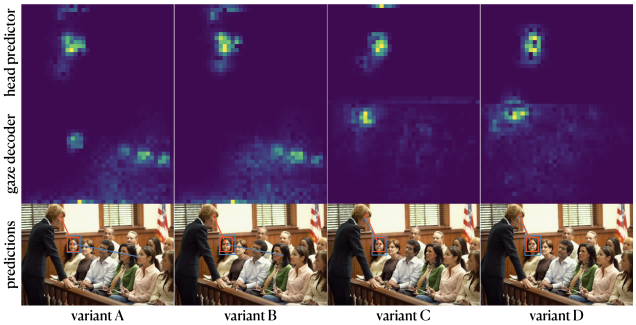


Figure 5. Visualization of the cross-attention maps of the human head predictor and gaze queries of GazeDETR variants A to D. The predictions (blue) and ground truth (orange) are also shown.

Backbone. There was only a minimal increase in performance when ResNet101 was used, with *AUC* 0.953, *Avg. Dist.* 0.099, *Min. Dist.* 0.054 and *mAP* 0.549.

4.5. Qualitative Analysis

4.5.1. Cross-attention maps of the decoders

In this section, the query slots associated with positive predictions are analyzed. The cross-attention maps are then taken from the last layers of the human head predictor and gaze decoder. Finally, the average value of the multi-attention heads is computed and visualized.

GazeDETR variants. As shown in Figure 5 (first row), the cross-attention maps of the head predictor are localized around the identified human heads, regardless of the GazeDETR variant. However, the cross-attention maps of their gaze decoders differ immensely, as shown in Figure 5 (second row). Removing the GSFE altered the ability of variants A and B to effectively utilize relevant visual context. As depicted in Figure 5 (third row), their gaze decoders attended to the right portion of the image, resulting in incorrect gaze predictions. This further explains their lower mAP performance. The addition of GSFE to variants C and D allowed them to more effectively exploit long-range dependencies to correctly identify the gaze target. More qualitative comparisons of GazeDETR variants are provided in the Supplementary Material.



Figure 6. Cross-attention maps of the human head predictor and gaze decoder. The predictions (blue) and ground truth (orange) are also shown. More examples are provided in the Supplementary Material.

The GazeDETR variants B and C that did not take advantage of the learned queries of the head predictor for their gaze decoders tended to depend less on head information, as their cross-attention maps showed less prominent values around the predicted head regions in Figure 5 (second row).

GazeDETR variant D. Here, we present more results from the best-performing GazeDETR variant. As shown in Figure 6 (first row), the cross-attention maps generated by the head predictor are fairly localized inside the bounding boxes associated with the positive prediction of human heads. This clearly showcases the ability of GazeDETR to solely utilize local information for head localization. Unlike those shown in Figure 4, the attentive fields of GazeDETR are not limited to the extremities of the detected objects. We hypothesize that although the extremities are sufficient for a positive detection, GazeDETR learns to incorporate facial information to help the gaze decoder in gaze prediction.

As shown in Figure 6 (second row), the cross-attention maps generated by the gaze decoder highlight salient regions where the same predicted human heads could be looking at. This demonstrates that the gaze decoder incorporates global information for gaze prediction. It is also evident that the gaze decoder attends to a more localized area of the human head (*e.g.*, eye region) associated with the positive predictions. We attribute this behavior to the specific reformulation of the cross-attention layers to utilize the learned head queries when inferring the gaze directions.

4.5.2. Bounding box and gaze prediction

In Figure 6 (last row), we present the bounding box and gaze point locations predicted by GazeDETR. We also present several qualitative examples of successful and missed predictions of GazeDETR in the supplementary material. Results on images with different numbers of humans are presented to showcase GazeDETR's performance on human head localization and associated gaze location prediction.

4.5.3. Limitations

GazeDETR occasionally fails at predicting the gaze directions in challenging scenarios, such as slightly occluded eye regions, conflicting eye and head directions and small heads in the image. More examples are provided in the Supplementary Material. We hypothesize that this is due to the fact that GazeDETR implicitly learns to encode both eye and head information to determine the gaze direction. One potential improvement is to add explicit supervision using eye information to disentangle eye and head directions.

5. Conclusion

In this work, we presented GazeDETR, a new transformer-based architecture for end-to-end gaze target detection. Prior works highlighted the issue of long training times and slow convergence of transformer-based models for gaze detection. One potential explanation is that their unified decoders learn entangled representations for the joint detection of head locations and their gaze directions. Since the former requires local information and the latter requires both local and global information, long training schedules are required to learn coherent attention. GazeDETR addresses these challenges by learning disentangled representations that allow for the generation of attentive fields consistent for each subtask. We performed extensive ablation studies to gain a better understanding of the key model components. Despite being end-to-end, GazeDETR achieves new state-of-the-art results on different datasets. Notably, it achieves better performance than models that rely on head annotations and off-the-shelf head detectors.

References

[1] Henny Admoni and Brian Scassellati. Social eye gaze in human-robot interaction: a review. *Journal of Human-Robot Interaction*, 6(1):25–63, 2017. 1

[2] Jun Bao, Buyu Liu, and Jun Yu. Escnet: Gaze target detection with the understanding of 3d scenes. In *Proceedings of the IEEE/CVF Conference on Computer Vision and Pattern Recognition*, pages 14126–14135, 2022. 2, 6

[3] Nicolas Carion, Francisco Massa, Gabriel Synnaeve, Nicolas Usunier, Alexander Kirillov, and Sergey Zagoruyko. End-to-end object detection with transformers. In *European conference on computer vision*, pages 213–229. Springer, 2020. 2, 3, 4

[4] Eunji Chong, Nataniel Ruiz, Yongxin Wang, Yun Zhang, Agata Rozga, and James M Rehg. Connecting gaze, scene, and attention: Generalized attention estimation via joint modeling of gaze and scene saliency. In *Proceedings of the European conference on computer vision (ECCV)*, pages 383–398, 2018. 1, 2, 6

[5] Eunji Chong, Yongxin Wang, Nataniel Ruiz, and James M Rehg. Detecting attended visual targets in video. In *Proceedings of the IEEE/CVF conference on computer vision and pattern recognition*, pages 5396–5406, 2020. 1, 2, 4, 5, 6

[6] Ryan Anthony de Belen, Gelareh Mohammadi, and Arcot Sowmya. Temporal understanding of gaze communication with gazetransformer. In *NeuRIPS 2023 Workshop on Gaze Meets ML*, 2023. 1, 2, 3

[7] Ryan Anthony J De Belen, Tomasz Bednarz, Arcot Sowmya, and Dennis Del Favero. Computer vision in autism spectrum disorder research: a systematic review of published studies from 2009 to 2019. *Translational psychiatry*, 10(1):333, 2020. 1

[8] Lifeng Fan, Yixin Chen, Ping Wei, Wenguan Wang, and Song-Chun Zhu. Inferring shared attention in social scene videos. In *Proceedings of the IEEE conference on computer vision and pattern recognition*, pages 6460–6468, 2018. 1

[9] Yi Fang, Jiapeng Tang, Wang Shen, Wei Shen, Xiao Gu, Li Song, and Guangtao Zhai. Dual attention guided gaze target detection in the wild. In *Proceedings of the IEEE/CVF conference on computer vision and pattern recognition*, pages 11390–11399, 2021. 2, 6

[10] Xavier Glorot and Yoshua Bengio. Understanding the difficulty of training deep feedforward neural networks. In *Proceedings of the thirteenth international conference on artificial intelligence and statistics*, pages 249–256. JMLR Workshop and Conference Proceedings, 2010. 5

[11] Anshul Gupta, Samy Tafasca, and Jean-Marc Odobez. A modular multimodal architecture for gaze target prediction: Application to privacy-sensitive settings. In *Proceedings of the IEEE/CVF Conference on Computer Vision and Pattern Recognition*, pages 5041–5050, 2022. 2, 6

[12] Kaiming He, Xiangyu Zhang, Shaoqing Ren, and Jian Sun. Deep residual learning for image recognition. In *Proceedings of the IEEE conference on computer vision and pattern recognition*, pages 770–778, 2016. 5

[13] Zhengxi Hu, Kunxu Zhao, Bohan Zhou, Hang Guo, Shichao Wu, Yuxue Yang, and Jingtai Liu. Gaze target estimation inspired by interactive attention. *IEEE Transactions on Circuits and Systems for Video Technology*, 32(12):8524–8536, 2022. 6

[14] Tianlei Jin, Zheyuan Lin, Shiqiang Zhu, Wen Wang, and Shunda Hu. Multi-person gaze-following with numerical coordinate regression. In *2021 16th IEEE International Conference on Automatic Face and Gesture Recognition (FG 2021)*, pages 01–08. IEEE, 2021. 2, 6

[15] Tianlei Jin, Qizhi Yu, Shiqiang Zhu, Zheyuan Lin, Jie Ren, Yuanhai Zhou, and Wei Song. Depth-aware gaze-following via auxiliary networks for robotics. *Engineering Applications of Artificial Intelligence*, 113:104924, 2022. 1, 2, 6

[16] Harold W Kuhn. The hungarian method for the assignment problem. *Naval research logistics quarterly*, 2(1-2):83–97, 1955. 4

[17] Jing Li, Zejin Chen, Yihao Zhong, Hak-Keung Lam, Junxia Han, Gaoxiang Ouyang, Xiaoli Li, and Honghai Liu. Appearance-based gaze estimation for asd diagnosis. *IEEE Transactions on Cybernetics*, 52(7):6504–6517, 2022. 1

[18] Dongze Lian, Zehao Yu, and Shenghua Gao. Believe it or not, we know what you are looking at! In *Asian Conference on Computer Vision*, pages 35–50. Springer, 2018. 2, 6

[19] Zhi-Yi Lin, Jouh Yeong Chew, Jan van Gemert, and Xucong Zhang. Gazehta: End-to-end gaze target detection with head-target association. *arXiv preprint arXiv:2404.10718*, 2024. 1

[20] Shilong Liu, Feng Li, Hao Zhang, Xiao Yang, Xianbiao Qi, Hang Su, Jun Zhu, and Lei Zhang. Dab-detr: Dynamic anchor boxes are better queries for detr. *arXiv preprint arXiv:2201.12329*, 2022. 2, 3

[21] I Loshchilov. Decoupled weight decay regularization. *arXiv preprint arXiv:1711.05101*, 2017. 5

[22] Depu Meng, Xiaokang Chen, Zejia Fan, Gang Zeng, Houqiang Li, Yuhui Yuan, Lei Sun, and Jingdong Wang. Conditional detr for fast training convergence. In *Proceedings of the IEEE/CVF international conference on computer vision*, pages 3651–3660, 2021. 2, 3, 4

[23] Adria Recasens, Aditya Khosla, Carl Vondrick, and Antonio Torralba. Where are they looking? *Advances in neural information processing systems*, 28, 2015. 1, 2, 4, 5, 6

[24] Samy Tafasca, Anshul Gupta, Nada Kojovic, Mirko Gelsomini, Thomas Maillart, Michela Papandrea, Marie Schaer, and Jean-Marc Odobez. The ai4autism project: A multimodal and interdisciplinary approach to autism diagnosis and stratification. In *Companion Publication of the 25th International Conference on Multimodal Interaction*, pages 414–425, 2023. 1

[25] Samy Tafasca, Anshul Gupta, and Jean-Marc Odobez. Childplay: A new benchmark for understanding children's gaze behaviour. In *Proceedings of the IEEE/CVF International Conference on Computer Vision*, pages 20935–20946, 2023. 1, 2, 4, 6

[26] Samy Tafasca, Anshul Gupta, and Jean-Marc Odobez. Sharingan: A transformer architecture for multi-person gaze following. In *Proceedings of the IEEE/CVF Conference*

on Computer Vision and Pattern Recognition, pages 2008–2017, 2024. 1, 2, 6

[27] Francesco Tonini, Cigdem Beyan, and Elisa Ricci. Multimodal across domains gaze target detection. In *Proceedings of the 2022 International Conference on Multimodal Interaction*, pages 420–431, 2022. 6

[28] Francesco Tonini, Nicola Dall'Asen, Cigdem Beyan, and Elisa Ricci. Object-aware gaze target detection. In *Proceedings of the IEEE/CVF International Conference on Computer Vision*, pages 21860–21869, 2023. 2

[29] Danyang Tu, Xiongkuo Min, Huiyu Duan, Guodong Guo, Guangtao Zhai, and Wei Shen. End-to-end human-gaze-target detection with transformers. In *2022 IEEE/CVF Conference on Computer Vision and Pattern Recognition (CVPR)*, pages 2192–2200. IEEE, 2022. 1, 2, 3, 5, 6

GazeDETR: Gaze Detection using Disentangled Head and Gaze Representations

Supplementary Material

Some figures in the main paper are too small to view normally. To improve visibility and readability, we enlarged and/or rearranged the contents of Figure 1, Figure 2, Figure 3, Figure 4 and Figure 5 and kept the same figure numbers as in the main paper.

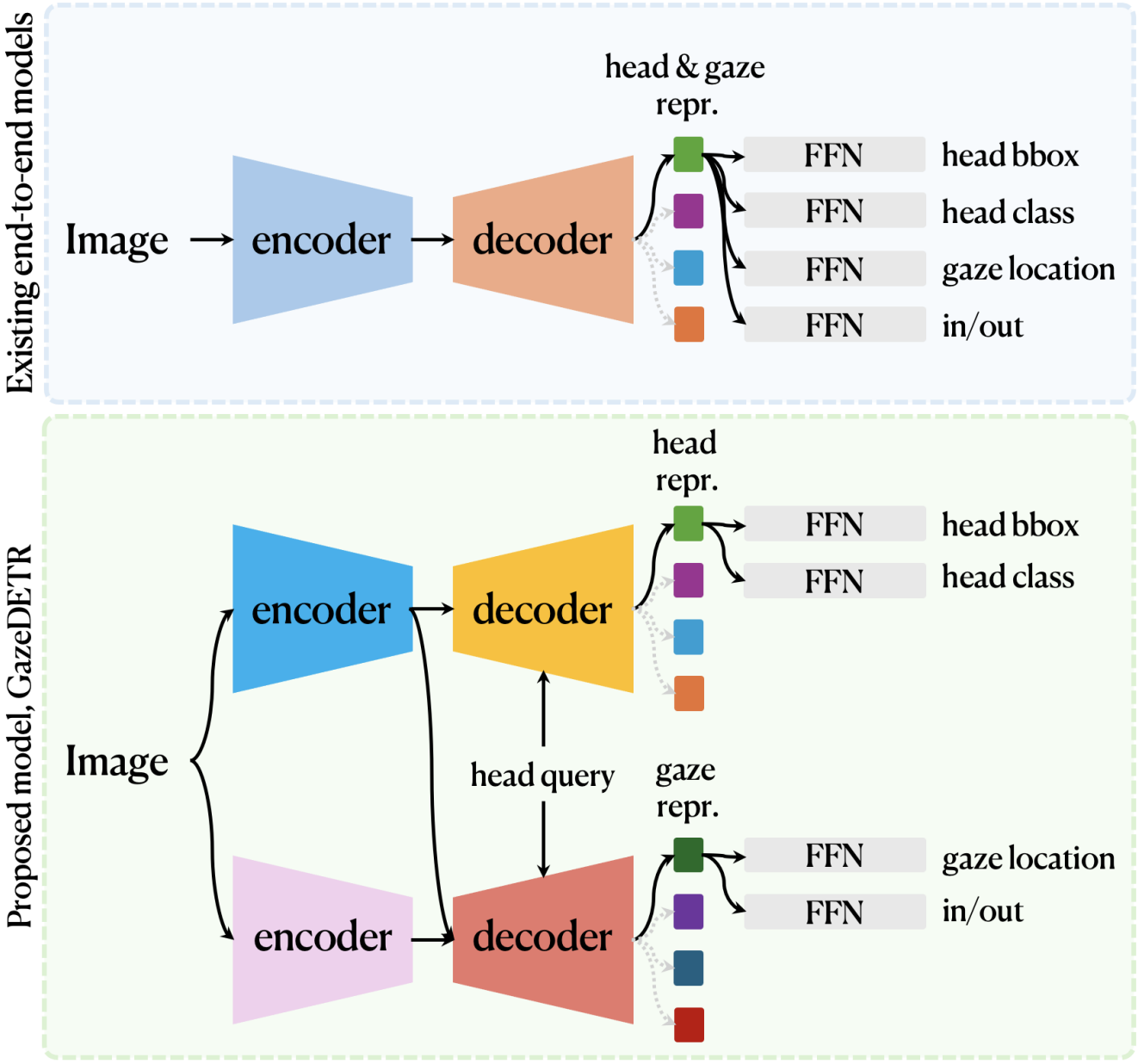


Figure 1. Comparison of existing approaches and the proposed approach (GazeDETR) for end-to-end gaze target detection. *(top)* existing approaches learn a unified representation for human head localization and gaze target detection, while *(bottom)* GazeDETR learns disentangled representations for the two subtasks. A shared query is used to promote interactions between the two decoders.

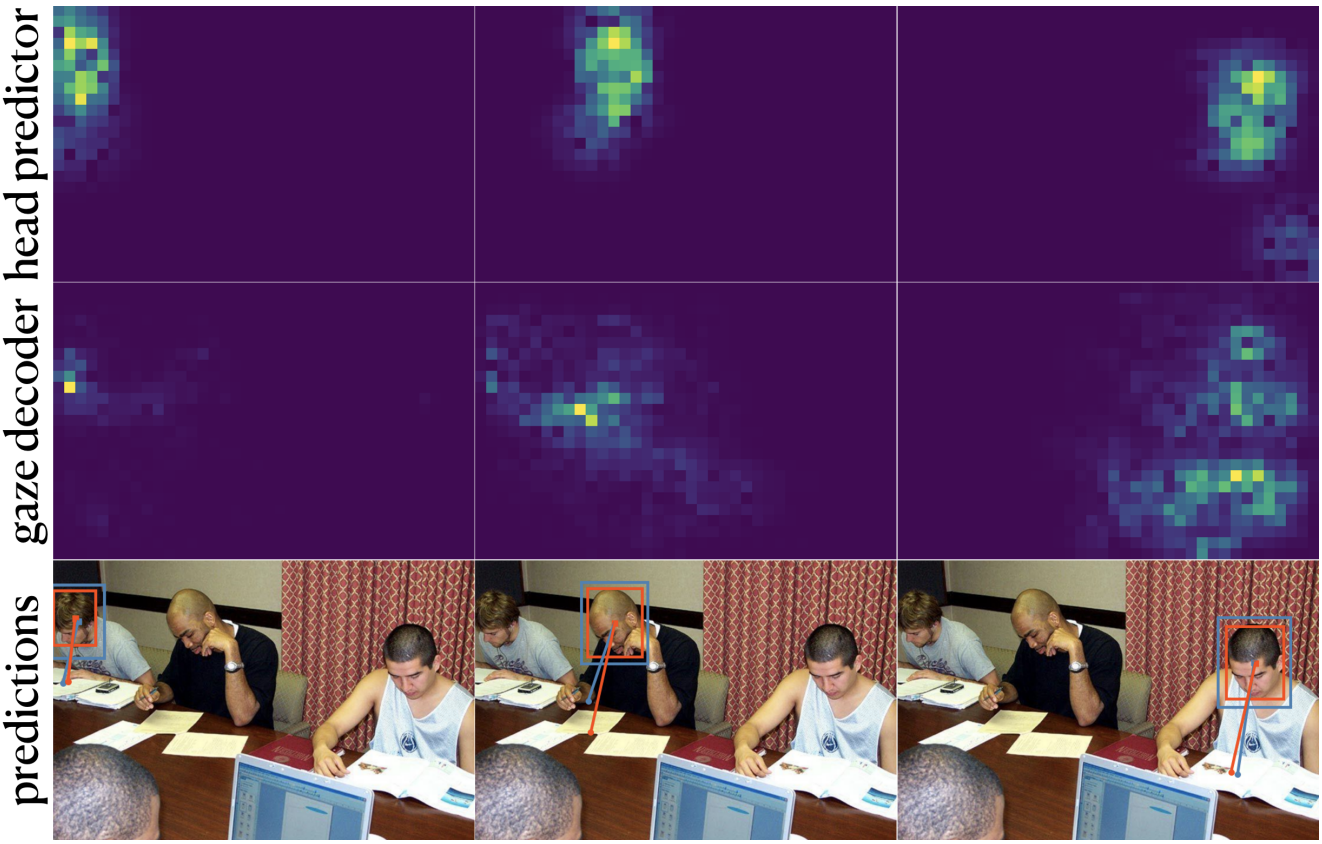


Figure 2. Cross-attention of the head predictor and gaze decoder. The predictions (blue) and ground truth (orange) are also shown.

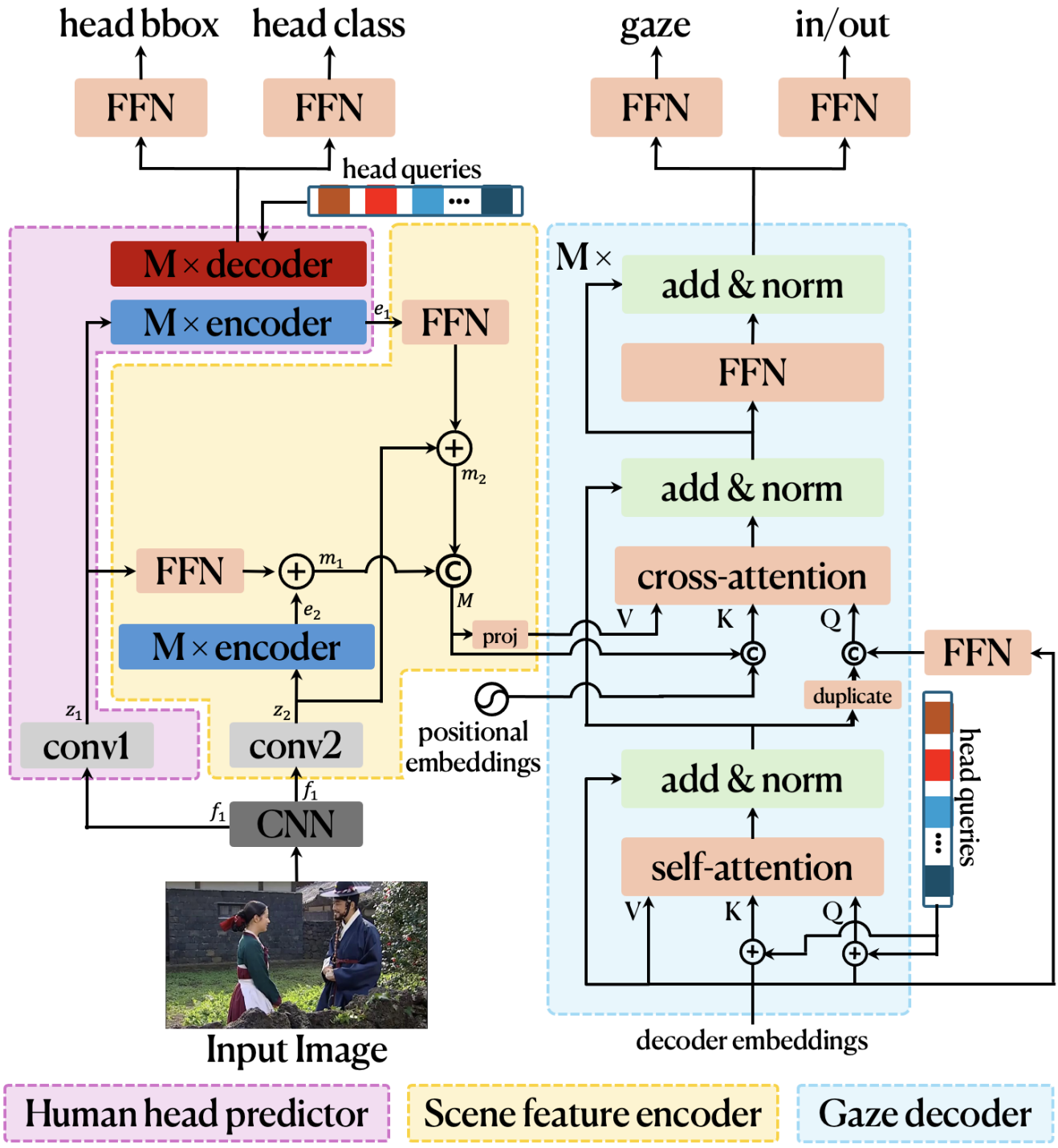


Figure 3. GazeDETR overview. The human head predictor extracts relevant features from the input image for head localization. Additional contextual information is extracted using the scene feature encoder and used by the gaze decoder for gaze prediction.

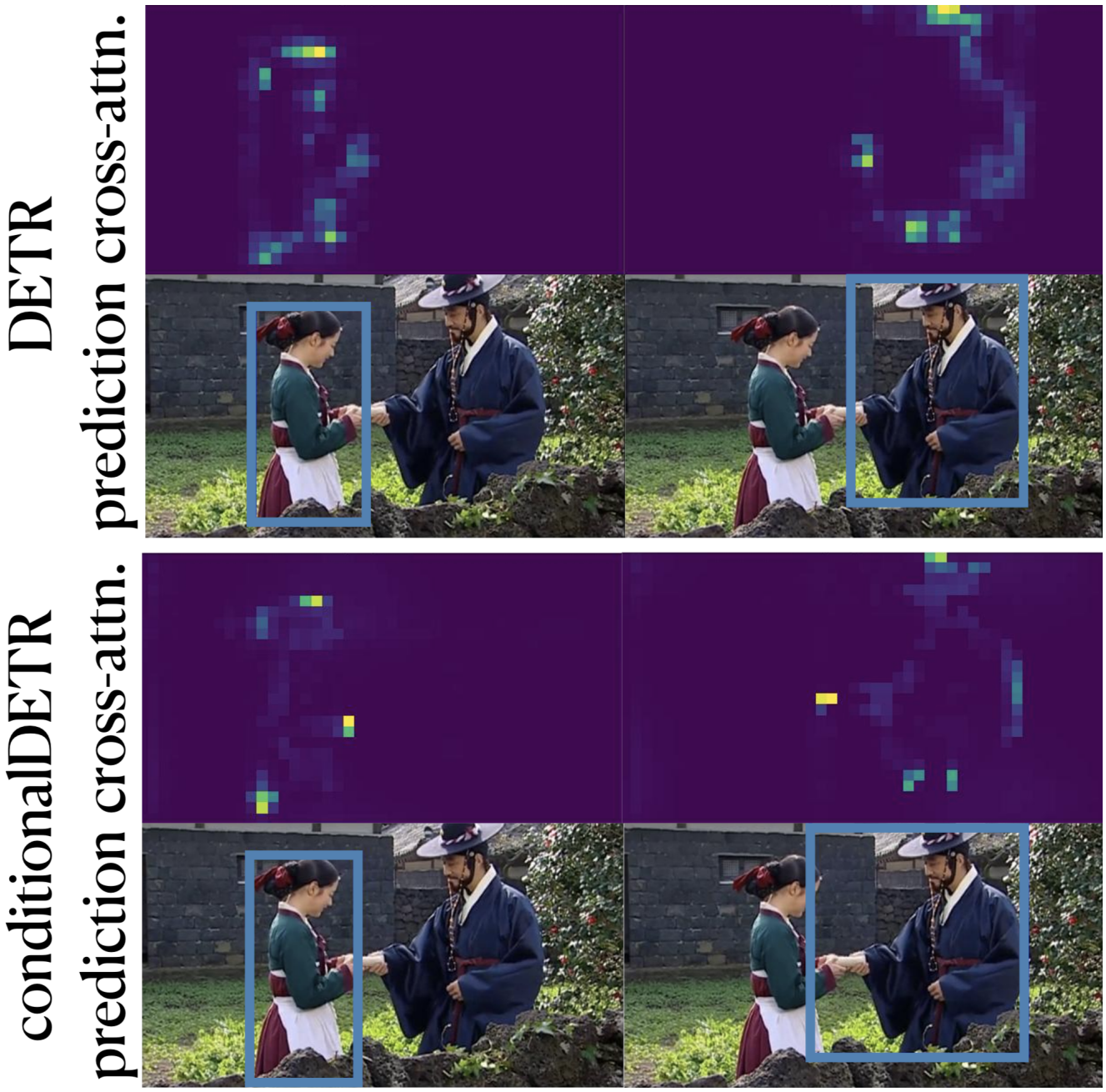


Figure 4. Visualization of the cross-attention maps of DETR architectures. Both DETR [3] and conditionalDETR [22] generate maps that highlight the extremities of the detected objects.

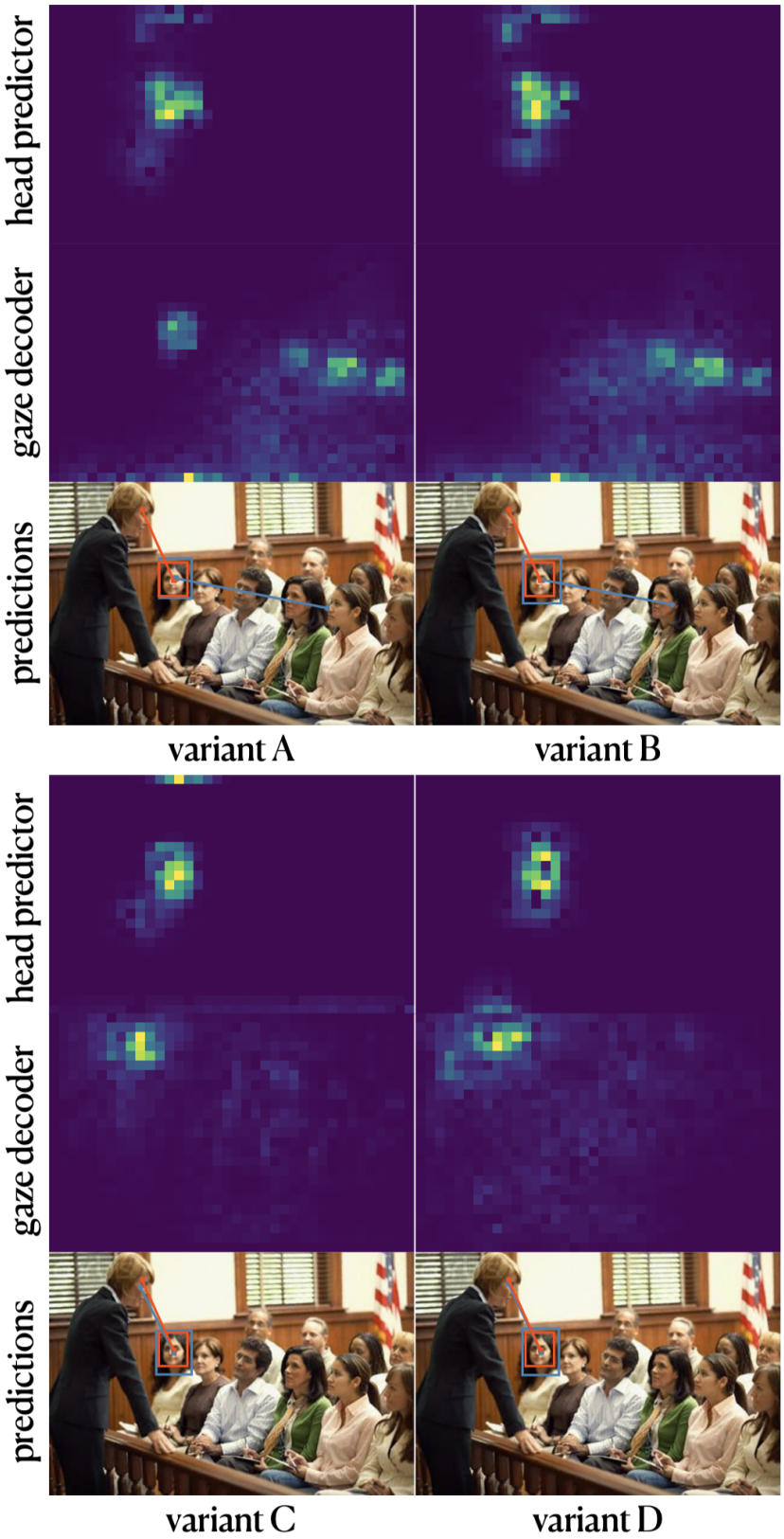


Figure 5. Visualization of the cross-attention maps of the human head predictor and gaze queries of GazeDETR variants A to D. The predictions (blue) and ground truth (orange) are also shown.

1. Implementation Details

We initially train GazeDETR on *GazeFollow* for 50 epochs and fine-tune on either *VideoAttentionTarget* or *ChildPlay* for 20 epochs. We will release our training and inference codes, as well as the model checkpoints.

2. GazeDETR variants

Figure 6 provides a more detailed overview of the different module components of the GazeDETR variants. Note that the GazeDETR variants A and B do not include the Global Scene Feature Encoder (GSFE). As a result, their gaze decoders utilize the embedding output, e, of the encoder of GSFE for their memory. Since GazeDETR variants C and D include the GSFE, their gaze decoder memory is a fusion of features, M, learned by the human head predictor and scene feature encoder. For the matrix multiplication to be valid in their cross-attention layers, M is projected to a lower dimension during Value formation while the self-attention output is duplicated during Query formation.

Note the difference between the queries used by the gaze decoders of the gazeDETR variants. GazeDETR variants A and D utilize the head queries learned by the head predictor, while GazeDETR variants B and C learn new gaze queries. As a result, they require fewer number of parameters.

Predictions of GazeDETR variants are shown in Figure 7 and Figure 8. As can be observed, the cross-attention maps of the head predictors are localized around the predicted human head, regardless of the GazeDETR variant. The cross-attention maps of the gaze decoders differ immensely, affecting the final gaze prediction. It is noticeable that GazeDETR variants A and B perform worse than C and D, proving the effectiveness of the GSFE module.

3. Quantitative Results

We show the cross-attention maps of the head predictor and the gaze decoder associated with positive predictions from our best-performing model, GazeDETR variant D. The predictions (blue) and ground truth (orange) are also shown. Bounding boxes denote locations of the head, while lines depict directions towards the predicted gaze location.

3.1. More Results on *GazeFollow*

We show extensive predictions of GazeDETR variant D on *GazeFollow* in Figure 9, Figure 10 and Figure 11.

3.2. More Results on *VideoAttentionTarget*

We show extensive predictions of GazeDETR variant D on *VideoAttentionTarget* in Figure 12, Figure 13 and Figure 14.

3.3. More Results on *ChildPlay*

We show extensive predictions of GazeDETR variant D on *ChildPlay* in Figure 15, Figure 16, Figure 17.

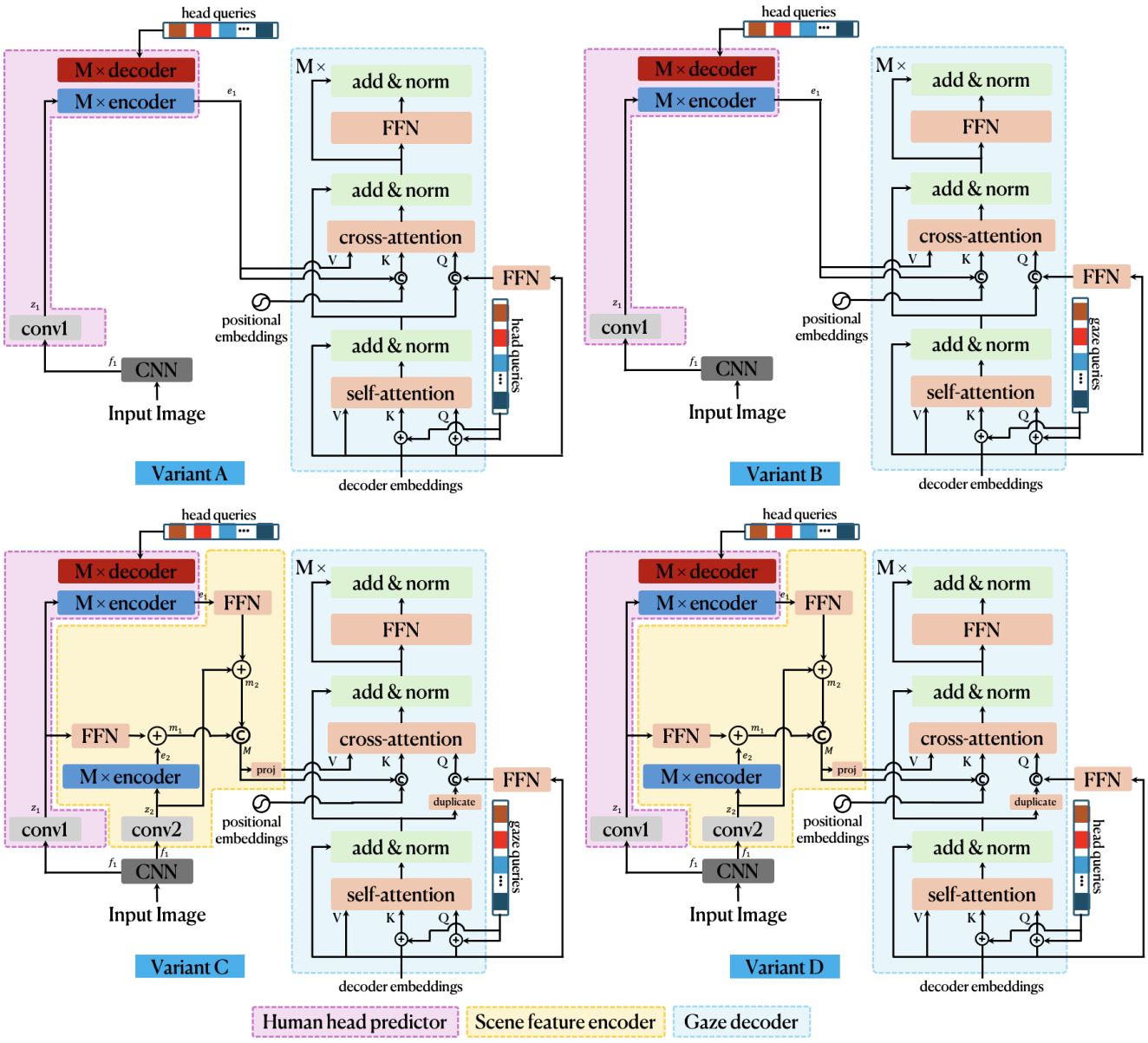


Figure 6. Comparison of GazeDETR variants with different module components.

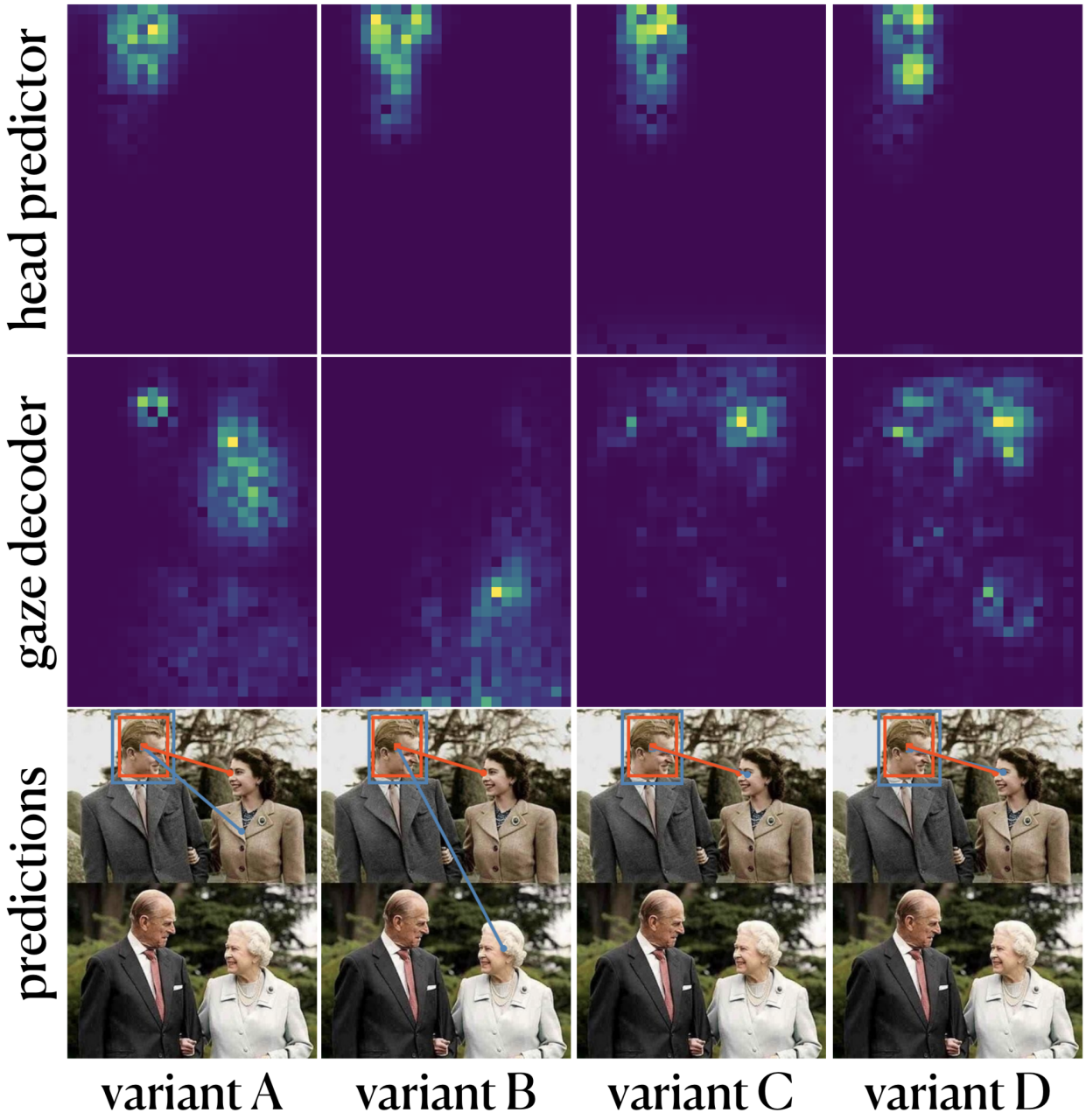


Figure 7. Visualization of the cross-attention maps of the human head predictor and gaze queries of GazeDETR variants A to D. The predictions (blue) and ground truth (orange) are also shown.

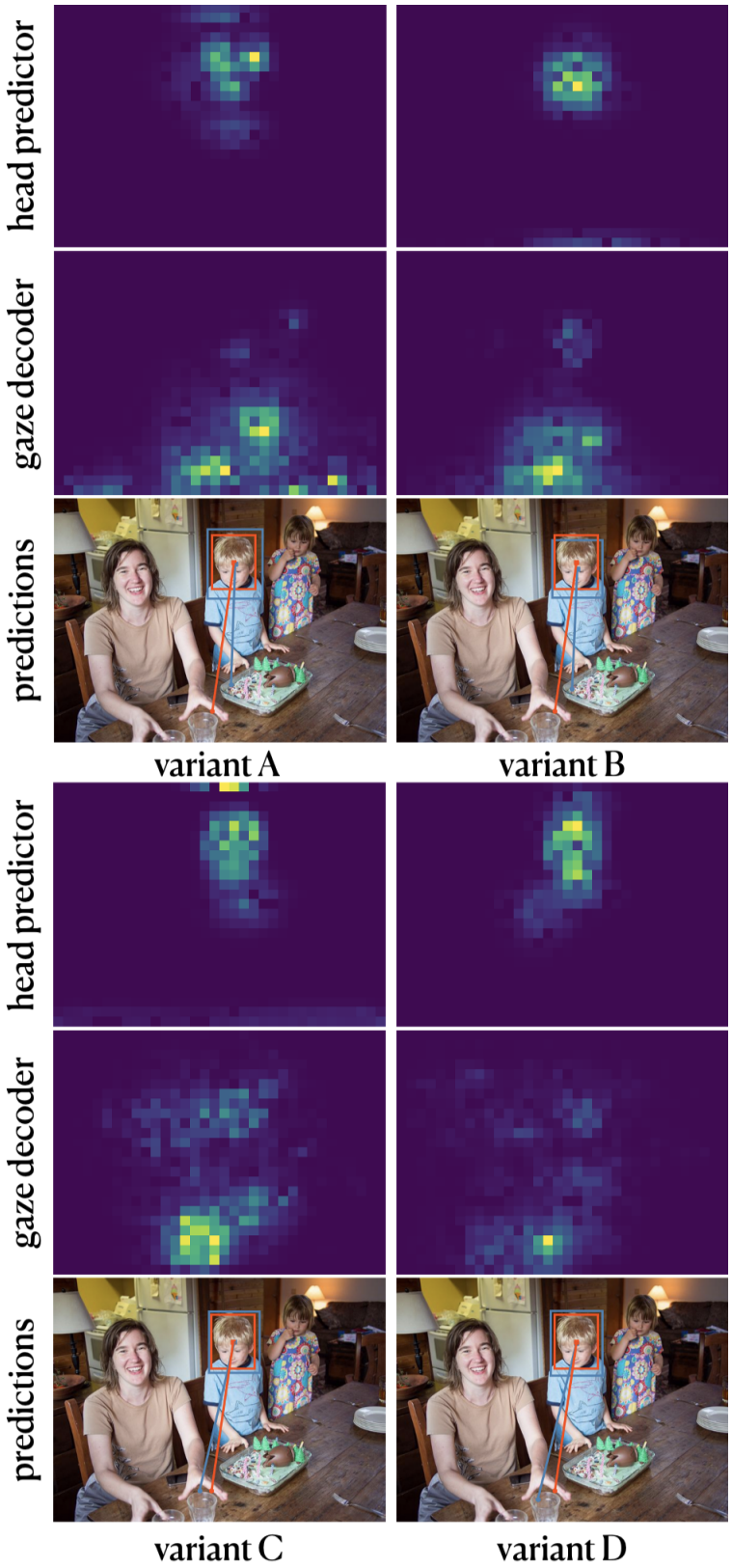


Figure 8. Visualization of the cross-attention maps of the human head predictor and gaze queries of GazeDETR variants A to D. The predictions (blue) and ground truth (orange) are also shown.

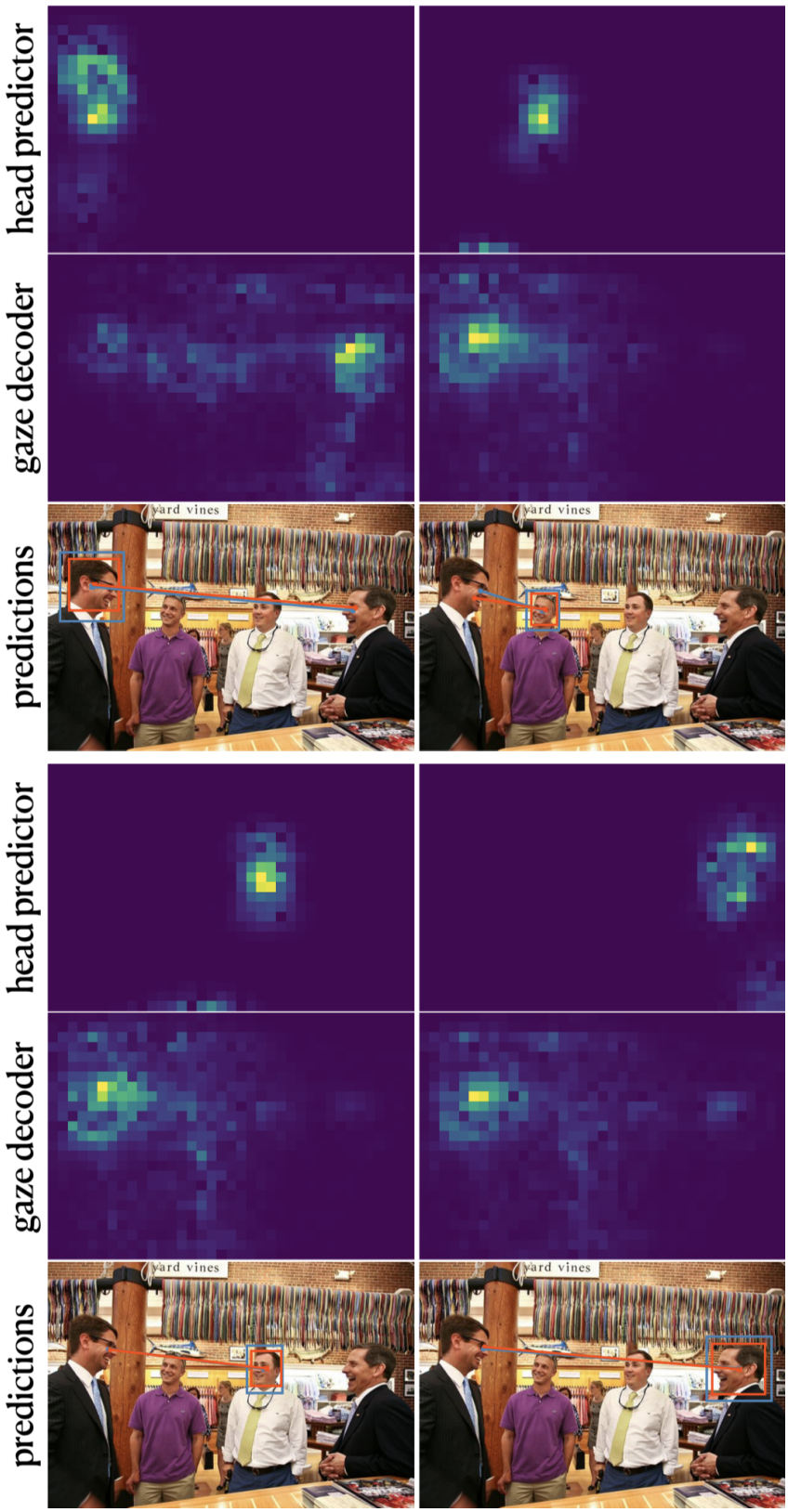


Figure 9. Visualization of the cross-attention maps of the human head predictor and gaze queries. The images are taken from *GazeFollow*. The predictions (blue) and ground truth (orange) are also shown.

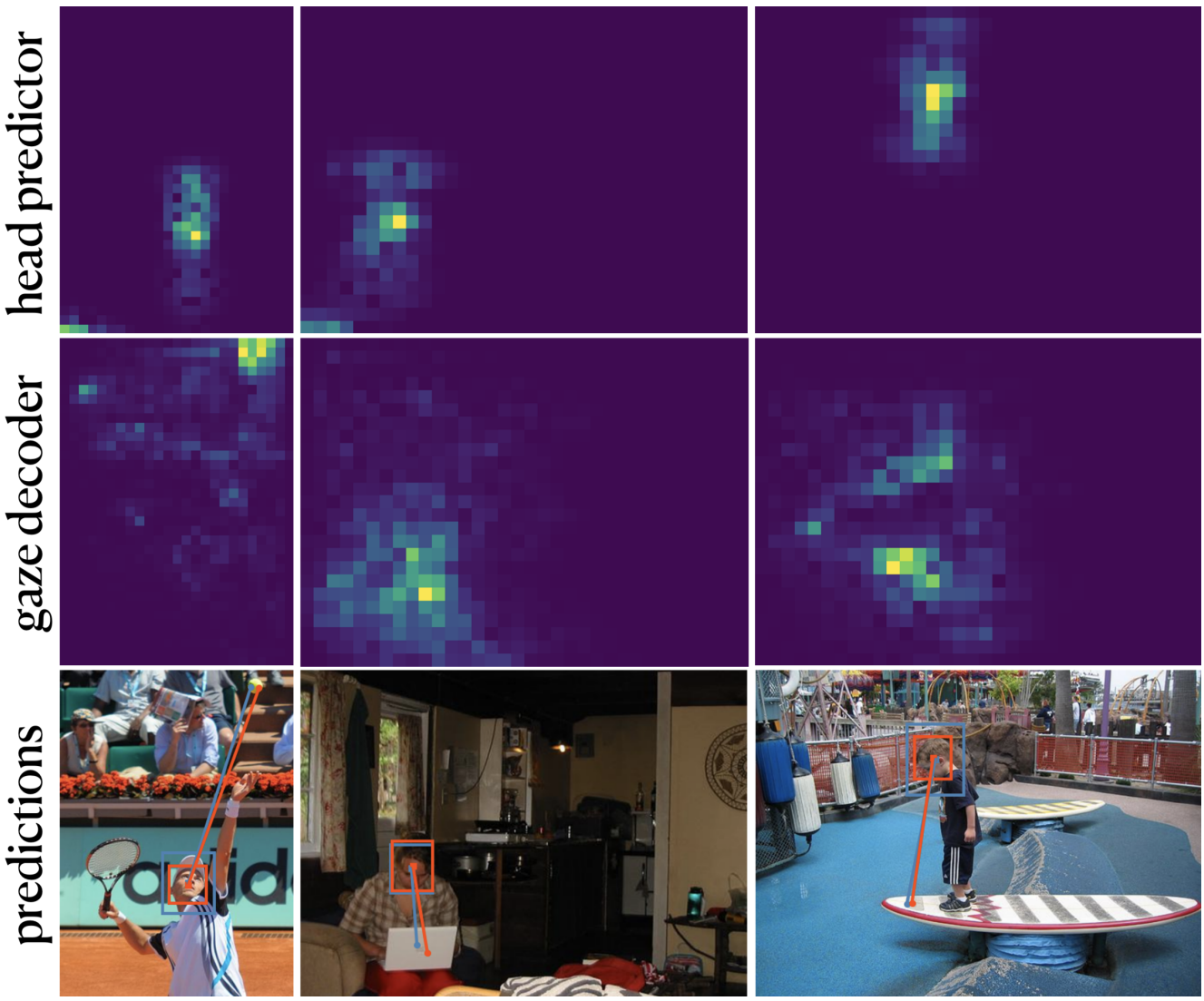


Figure 10. Visualization of the cross-attention maps of the human head predictor and gaze queries. The images are taken from *GazeFollow*. The predictions (blue) and ground truth (orange) are also shown.

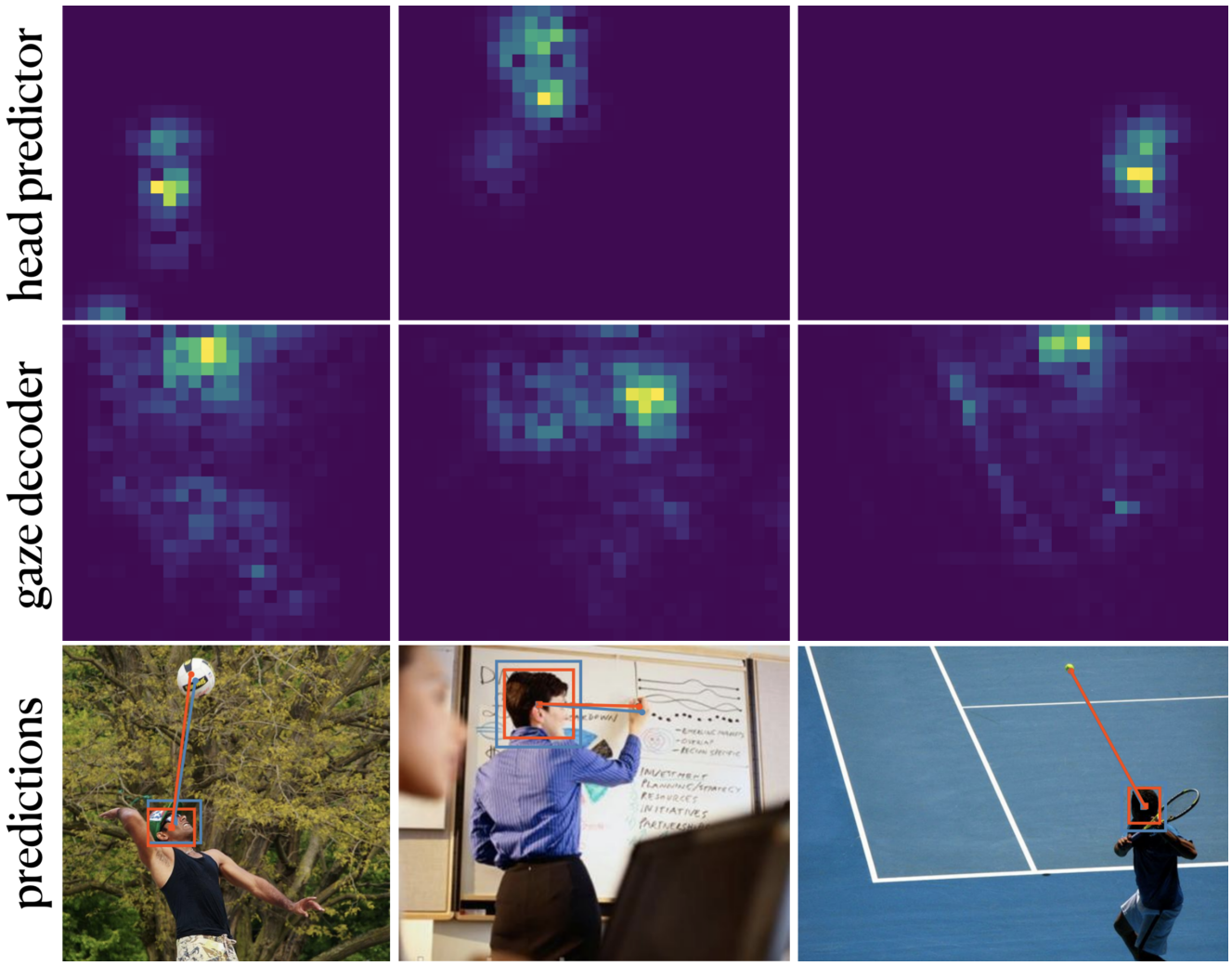


Figure 11. Visualization of the cross-attention maps of the human head predictor and gaze queries. The images are taken from *GazeFollow*. The predictions (blue) and ground truth (orange) are also shown.

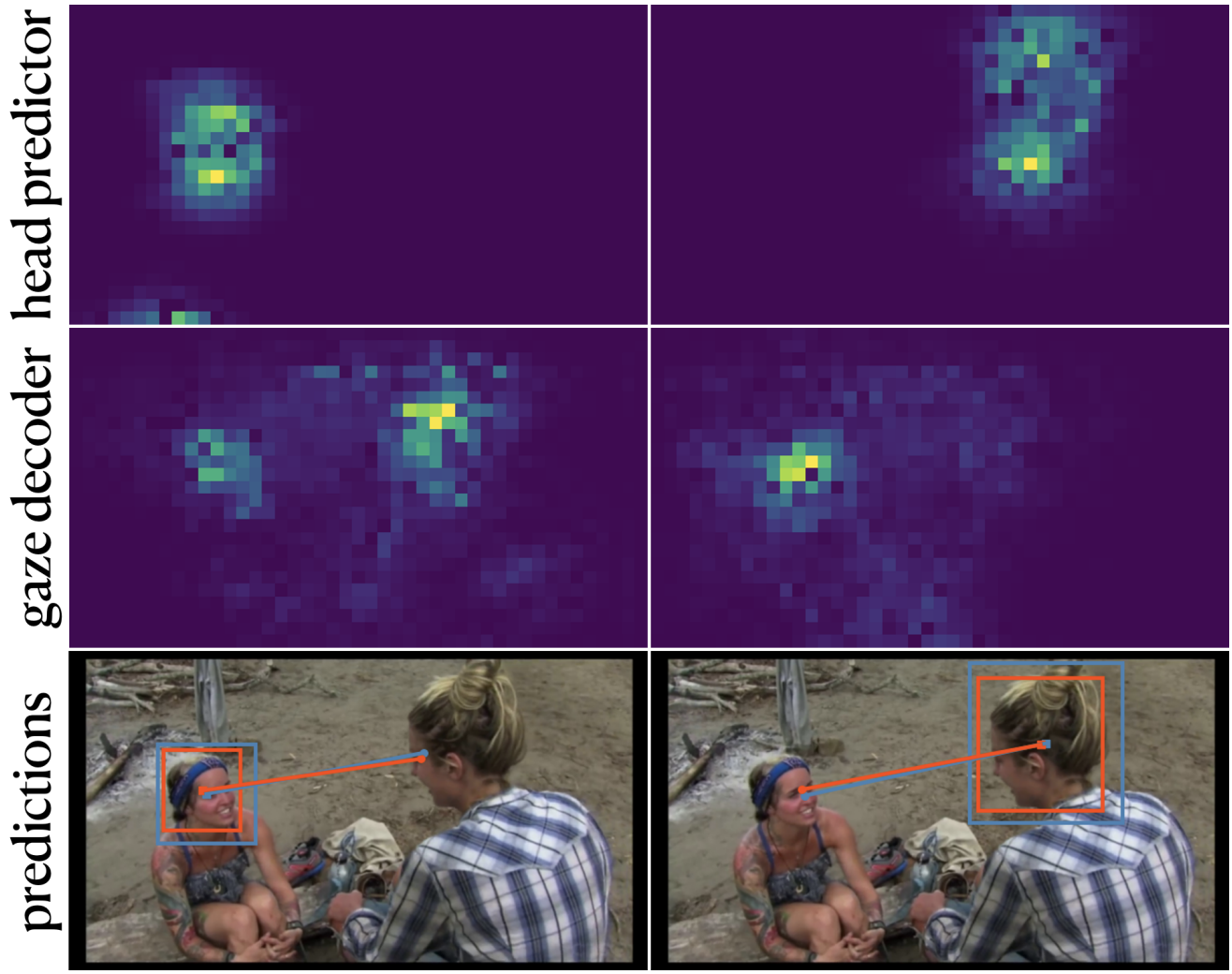


Figure 12. Visualization of the cross-attention maps of the human head predictor and gaze queries. The images are taken from *VideoAttentionTarget*. The predictions (blue) and ground truth (orange) are also shown.



Figure 13. Visualization of the cross-attention maps of the human head predictor and gaze queries. The images are taken from *VideoAttentionTarget*. The predictions (blue) and ground truth (orange) are also shown.

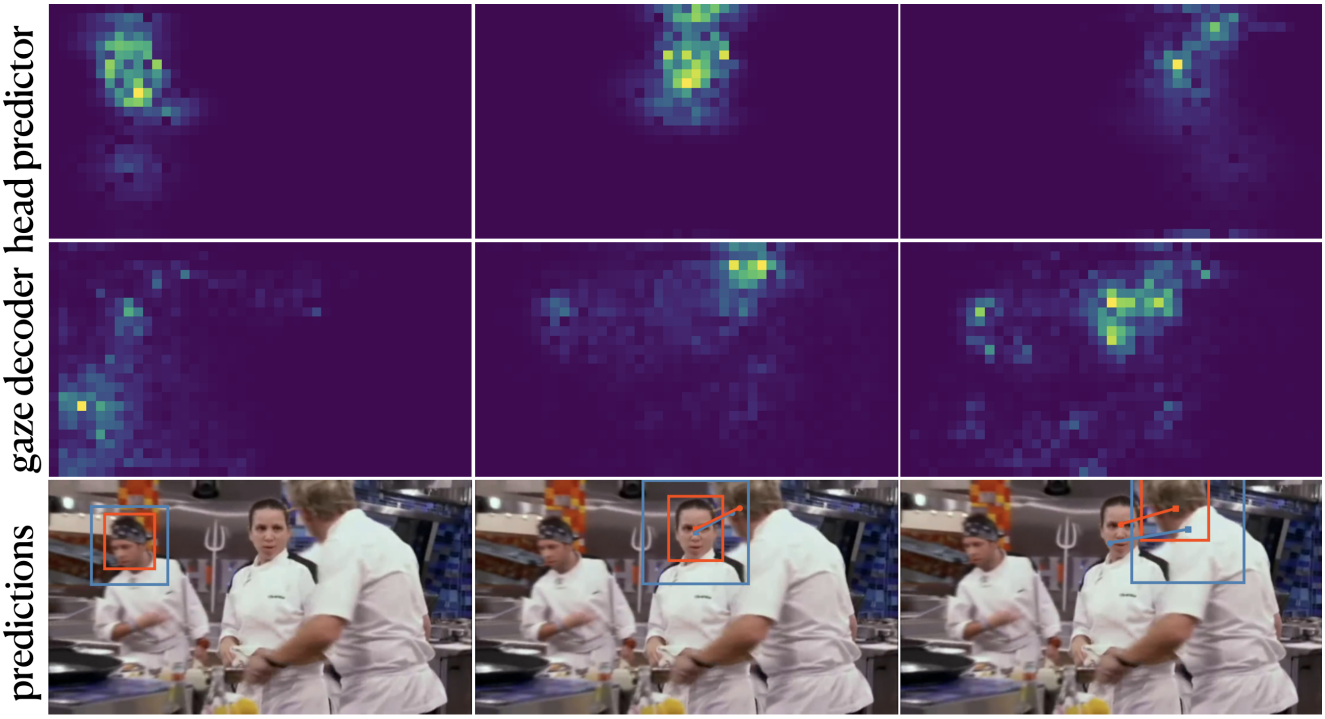


Figure 14. Visualization of the cross-attention maps of the human head predictor and gaze queries. The images are taken from *VideoAttentionTarget*. The predictions (blue) and ground truth (orange) are also shown.

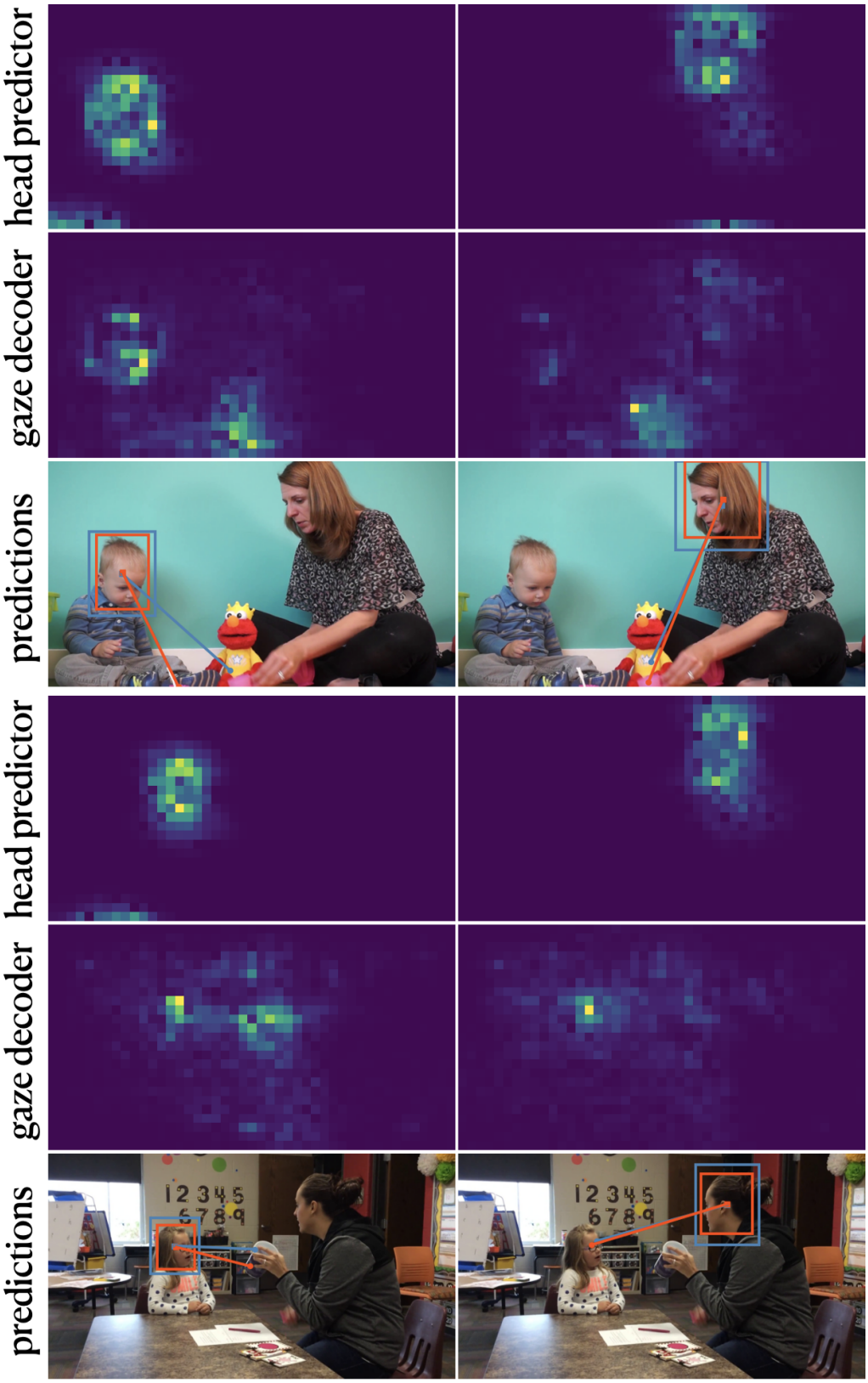


Figure 15. Visualization of the cross-attention maps of the human head predictor and gaze queries. The images are taken from *ChildPlay*. The predictions (blue) and ground truth (orange) are also shown.

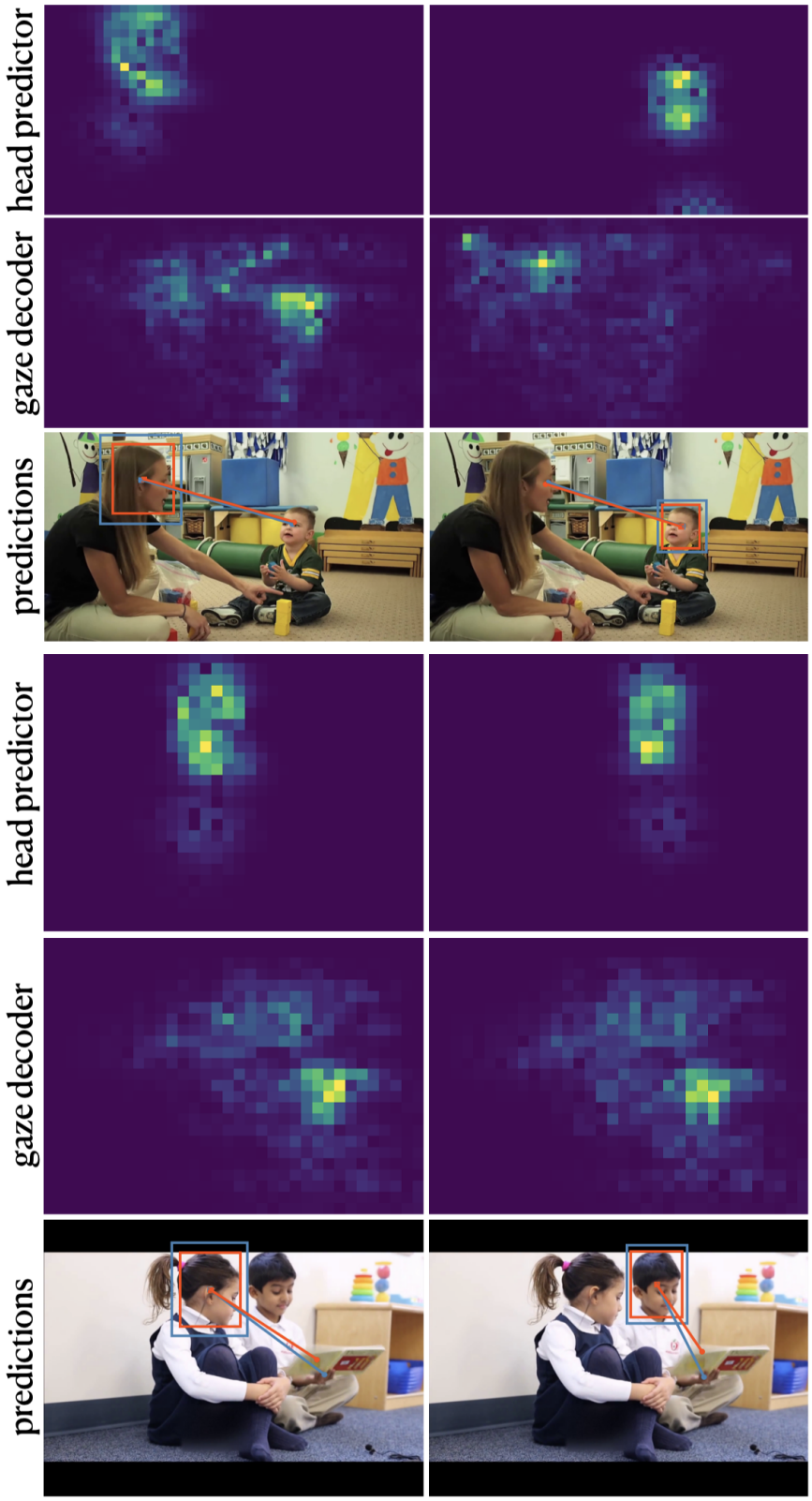


Figure 16. Visualization of the cross-attention maps of the human head predictor and gaze queries. The images are taken from *ChildPlay*. The predictions (blue) and ground truth (orange) are also shown.

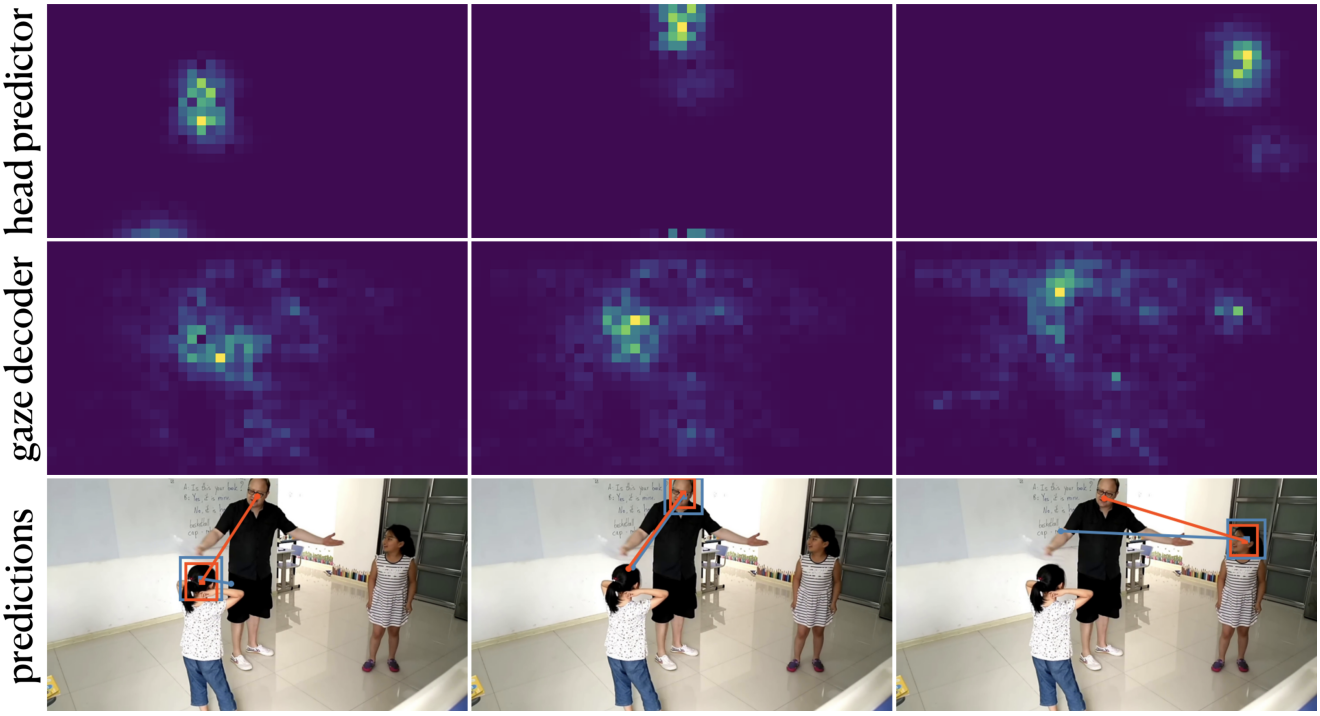


Figure 17. Visualization of the cross-attention maps of the human head predictor and gaze queries. The images are taken from *ChildPlay*. The predictions (blue) and ground truth (orange) are also shown.